Nanotechnology

PAPER

The impact of oxygen vacancy defect density on the nonlinearity and short-term plasticity of TiO_2-based exponential selector

To cite this article: Mun Yin Chee *et al* 2023 *Nanotechnology* **34** 365201

View the article online for updates and enhancements.

You may also like

- Effect of graphene intercalation on nonlinearity of Ag/quartz/Pt selector: first-principle calculations
Yuehua Dai, Xiaoxiao Chen, Fei Tao et al.

- Resistive switching memory for high density storage and computing
Xiao-Xin Xu, , Qing Luo et al.

- Effect of doping on the GR/MoS_2/GR selector: first-principle calculations
Yuehua Dai, Xing Li, Bin Yang et al.

This content was downloaded from IP address 3.0.220.147 on 19/06/2023 at 14:24

IOP Publishing

Nanotechnology

Nanotechnology **34** (2023) 365201 (8pp)

https://doi.org/10.1088/1361-6528/acda40

The impact of oxygen vacancy defect density on the nonlinearity and short-term plasticity of TiO_2-based exponential selector

Mun Yin Chee, Putu Andhita Dananjaya, Gerard Joseph Lim, Calvin Xiu Xian Lee, Lingli Liu and Wen Siang Lew

School of Physical and Mathematical Sciences, Nanyang Technological University, 21 Nanyang Link, 637371, Singapore

E-mail: wensiang@ntu.edu.sg

Received 20 April 2023, revised 22 May 2023
Accepted for publication 31 May 2023
Published 19 June 2023

Abstract

The readout margin of the one selector-one RRAM crossbar array architecture is strongly dependent on the nonlinearity of the selector device. In this work, we demonstrated that the nonlinearity of $Pt/TiO_2/Pt$ exponential selectors increases with decreasing oxygen vacancy defect density. The defect density is controlled by modulating the sputtering pressure in the oxide deposition process. Our results reveal that the dominant conduction mechanisms of the $Pt/TiO_2/Pt$ structure transit from Schottky emission to Poole–Frenkel emission with the increase of sputtering pressure. Such transition is attributed to the rise of oxygen vacancy concentration. In addition, the short-term plasticity feature of the $Pt/TiO_2/Pt$ selector is shown to be enhanced with a lower defect density. These results suggest that low defect density is necessary for improved exponential selector performances.

Supplementary material for this article is available online

Keywords: short-term plasticity, oxygen vacancy, TiO_2-based selector, 1S1R, RRAM

(Some figures may appear in colour only in the online journal)

1. Introduction

Hardware implementation of artificial neural networks (ANNs) has attracted extensive interest in the field of computing due to its promising performance in mimicking human brain capability [1, 2]. To emulate synaptic functionalities in the hardware ANNs, a non-volatile memory device with synaptic features is required. Among all the emerging and conventional memory devices, resistive random-access memory (RRAM), an emerging memory device, has been one of the most promising candidates to emulate synaptic functionalities due to its highly scalable device footprint ($\leqslant 4F^2$) and tunable characteristics [3]. To fully utilise the RRAM scalability potential, the RRAM device requires a compatible selection device, known as the selector, to work in tandem with it in a crossbar array configuration [4]. This is to mitigate the inherent sneak path current issue in highly connected crossbar array architecture. The sneak path current can be suppressed due to the highly nonlinear current–voltage (I–V) characteristics of the selector, and the readout margin of the crossbar array is strongly dependent on the I–V nonlinearity of the selector.

The nonlinearity is defined as the current ratio between the selector at a full-read voltage (V_{read}) and a half-read voltage ($V_{read}/2$) in the $V/2$ scheme. Several groups have proposed techniques to improve the nonlinearity of the exponential selectors, such as by creating an ultra-smooth bottom electrode [5], annealing at different temperatures [6] and varying the oxide thickness [7]. The nonlinearity of the selector is strongly influenced by the leakage current of the structure, and the leakage current may be affected by the oxygen vacancy defects in the dielectric layer. Therefore, it is of utmost importance to investigate the impact of oxygen vacancy defect density on the nonlinearity of the exponential selector; however, such a finding is still elusive.

 © 2023 IOP Publishing Ltd

A high nonlinearity of $>10^4$ was reported on TiO_x [8–11], TaO_x [5, 12, 13] and Co_3O_4-based [14] tunnelling selectors. Besides that, an amorphous ITZO-based selector was shown to achieve ~900 nonlinearity in the $V/3$ scheme after oxygen plasma treatment [15]. An ultrathin three-monolayer MoS_2-based tunnelling selector was also reported to achieve a low 25 nonlinearity value [16]. Nonetheless, the above-mentioned exponential selectors do not exhibit short-term plasticity features. The short-term plasticity feature is an important criterion to demonstrate temporal information processing capability in neuromorphic computing applications. Chao Du *et al* utilised the short-term plasticity of a WO_x-based dynamic memristor in a reservoir computing system to perform digit recognition [17]. In addition, in our previous work, the short-term plasticity of the $Pt/TiO_x/Pt$ exponential selector was demonstrated to enable the stimulation rate-dependent weight tuning in the one selector-one RRAM (1S1R) synapse [18]. Samuel Shin *et al* tuned the short-term plasticity of an organic mixed ionic-electronic conductor memristor by adding $LiClO_4$ salts [19]. Yewon Lee *et al* implemented both short-term and long-term memory in $Ag/HfO_2/SiO_2/Si$ memristor by controlling the strength of the applied signal [20]. However, the method of controlling the short-term plasticity of an exponential selector has not yet been reported.

In this work, we show that the nonlinearity and short-term plasticity of the $Pt/TiO_2/Pt$ selector can be tuned by modulating the oxygen vacancy defect density, which can be controlled via the sputtering pressure in the oxide deposition process. Additionally, the conduction mechanisms of the $Pt/TiO_2/Pt$ structures are demonstrated to be Schottky emission at low sputtering pressures (from 2 to 6 mTorr) and Poole–Frenkel emission at high sputtering pressure (9 mTorr). For sputtering pressure less than 6 mTorr, the Schottky barrier height (SBH) decreases with sputtering pressure. An explanation has been given to the SBH modification and transition from interface-limited to bulk-limited conduction mechanisms based on the increasing oxygen vacancy concentration with sputtering pressures.

2. Experimental methods

Exponential selectors comprising Pt(10 nm)/TiO_2(4 nm)/Pt (10 nm) were fabricated and patterned into 10 μm × 10 μm devices. Pt was deposited by using DC magnetron sputtering, while TiO_2 was deposited by RF magnetron sputtering at 50 W from a single TiO_2 target. In the fabrication process, the oxide and defect densities of the TiO_2 layer were controlled by modulating the sputtering pressure in the oxide deposition process. *I–V* measurements were conducted by using a Keithley 4200A-SCS semiconductor parameter analyser. In all the *I–V* measurements, a voltage bias was applied to the Pt TE while keeping the Pt BE grounded.

The density of the TiO_2 layers deposited under different sputtering pressures was determined by x-ray reflectometry (XRR) measurements, as shown in figure 1(a). The density of the films is calculated from the XRR measurement based on the Parratt formalism [21] and the theory of Nevot-Croce [22], as shown in the inset of figure 1(a). As the sputtering pressure increases, the density of the TiO_2 layers decreases. This result can be explained by the higher kinetic energy of the sputtered adatom at lower pressure due to the longer mean free path, which contributes to denser film growth [23–25]. Figure 1(b) shows the x-ray photoelectron spectroscopy (XPS) spectra of the TiO_2 layers for O 1s states with various sputtering pressures. The asymmetric O 1s peaks can be divided into two peaks, generally ascribed to the lattice oxygen (~529 eV) and the non-lattice oxygen (~530 eV) [26, 27]. The composition ratios of the non-lattice oxygen and conductive Ti^{3+} cations of the TiO_2 layers as a function of sputtering pressure are shown in figure 1(c). The composition ratios of the Ti^{3+} cations are extracted from the Ti 2p XPS spectra, as shown in the supplementary information (figure S1). As the sputtering pressure increases, the composition ratio of the non-lattice oxygen in the TiO_2 layers increases, which also indicates that the oxygen vacancy defect density increases. Higher sputtering pressure increases the number of collisions between the TiO_2 molecules and the Ar ions in the plasma, leading to weakly bonded O and more oxygen vacancy defects [28, 29]. Furthermore, as the sputtering pressure increases, the composition ratio of the Ti^{3+} cation increases, which agrees with the previous statement as the more conductive Ti^{3+} states are attributed to more oxygen vacancy defects. These results show that the oxide and defect densities of the TiO_2 layers are modulated by controlling the sputtering pressures. It is important to note that the Ti:O ratio is remained at 1:2 for all pressures based on the XPS results. Moreover, the x-ray diffraction results indicate that the TiO_2 films are amorphous from 2 to 9 mTorr sputtering pressures, as shown in the supplementary information (figure S2).

3. Results and discussion

A schematic illustration of the fabricated $Pt/TiO_2/Pt$ exponential selector is shown in figure 2(a). The inset in figure 2(a) shows the optical image of the 10 μm × 10 μm selector device. The *I–V* characteristics of the $Pt/TiO_2/Pt$ exponential selectors deposited under different sputtering pressures are shown in figure 2(b). At low voltage regions (-0.8 V $< V <$ 1 V), the measured current across the selector increases with sputtering pressure, which indicates that the leakage current at the off state of the selector increases with sputtering pressure. This increase in current is attributed to the increase in oxygen vacancy defect density in the TiO_2 film, as discussed in figure 1(c). At high positive voltage regions (V = 2 V), the measured current of the selector devices achieves ~200 and ~400 μA for sputtering pressures from 2 to 6 mTorr and 9 mTorr, respectively. On the other hand, at high negative voltage regimes ($V < -0.8$ V), the measured current across the selectors converges to the 2 mTorr device. The measured current of 3, 4 and 5 mTorr selectors converge to the 2 mTorr selector at -0.8 V, -1 V and -1.2 V, respectively. Figures 2(c) and (d) show the nonlinearity versus reading voltage of the selector in the $V/2$ scheme for positive

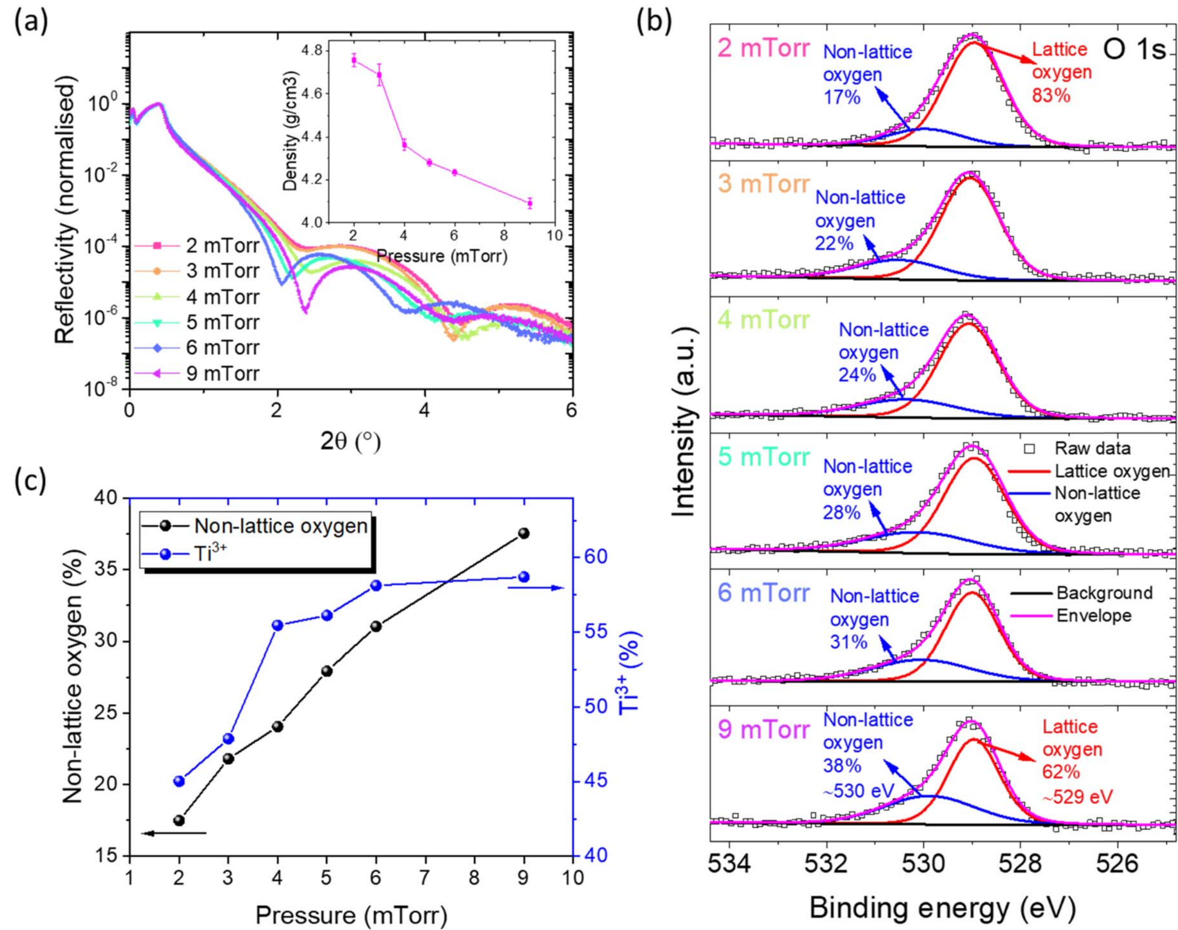

Figure 1. (a) XRR measurement of the 4 nm TiO_2 layer deposited under different sputtering pressures. Inset in (a) shows the density of the TiO_2 layer calculated from the XRR measurement. (b) XPS spectra of the TiO_2 layer for O 1s states with various sputtering pressures. (c) The non-lattice oxygen and conductive Ti^{3+} cation composition ratios of the TiO_2 layer as a function of sputtering pressure.

and negative voltage biases, respectively. The nonlinearity values are obtained from averages of five devices. At positive reading voltages, the nonlinearity of the selector increases when the pressure decreases over the entire voltage range. Whereas, at negative reading voltages, the nonlinearity is higher for lower pressure at the low and medium voltage regions ($-1.7\text{ V} < V_{\text{read}} < 0\text{ V}$), but at the high voltage region ($V_{\text{read}} < -1.7\text{ V}$), the nonlinearity of the 3 mTorr selector is the highest (∼300) and the nonlinearity of the 2 mTorr selector saturated at ∼270. The highest nonlinearity of the 3 mTorr device at $V_{\text{read}} < -1.7$ V can be ascribed to the overlapping of measured current with the 2 mTorr device at $V < -0.8$ V, as shown in figure 2(b). Additionally, the 4 mTorr achieves a high nonlinearity as 2 and 3 mTorr devices at 2 V because of the overlapping measured current at $V < -1$ V. The 3 mTorr selector achieves the highest nonlinearity of ∼300 at −1.9 V reading voltage, but at the other positive and negative reading voltage regions ($-1.7\text{ V} < V_{\text{read}} < 2\text{ V}$), 2 mTorr has the highest nonlinearity. Additionally, the nonlinearity in the $V/3$ scheme is obtained as shown in the supplementary information (figure S3). In the $V/3$ scheme, the nonlinearity of the selector increases with decreasing sputtering pressure over the full voltage range. The 2 mTorr device achieves ∼5000 and ∼1000 nonlinearity values at −1.98 V and 1.98 V reading voltage, respectively. Therefore, it is crucial to deposit the TiO_2 films at the lowest possible pressure in order to achieve the highest nonlinearity.

To understand the behaviour of electric charge carriers in the $Pt/TiO_2/Pt$ selector, several conduction mechanisms such as Schottky emission, Fowler–Nordheim tunnelling, direct tunnelling, Poole–Frenkel emission, space-charge-limited conduction and trap-assisted tunnelling are fitted to the *I–V* characteristics of the device. Among them, the Schottky emission fits well with the selectors from 2 to 6 mTorr ($R^2 > 0.99$), as shown in figure 3(a). The SBH, ϕ_B can be extracted from the fitting with the following equation [30–32]

$$J_{\text{SE}} = \frac{4\pi q m^* (kT)^2}{h^3} \exp\left[\frac{-q(\phi_B - \sqrt{qE/4\pi\varepsilon})}{kT}\right], \quad (1)$$

where $J_{\text{SE}} = I/A$ is the current density, A is the area of the device, $E = V/d$ is the electric field, d is the thickness of the oxide, and ε is the permittivity of the dielectric layer. The inset in figure 3(a) shows that the SBH decreases with increasing pressure until 6 mTorr. The selector with 9 mTorr sputtering pressure fits well with Poole–Frenkel emission ($R^2 > 0.99$) as compared to Schottky emission ($R^2 \approx 0.96$), as shown in figure 3(b). The current density of Poole–Frenkel emission can

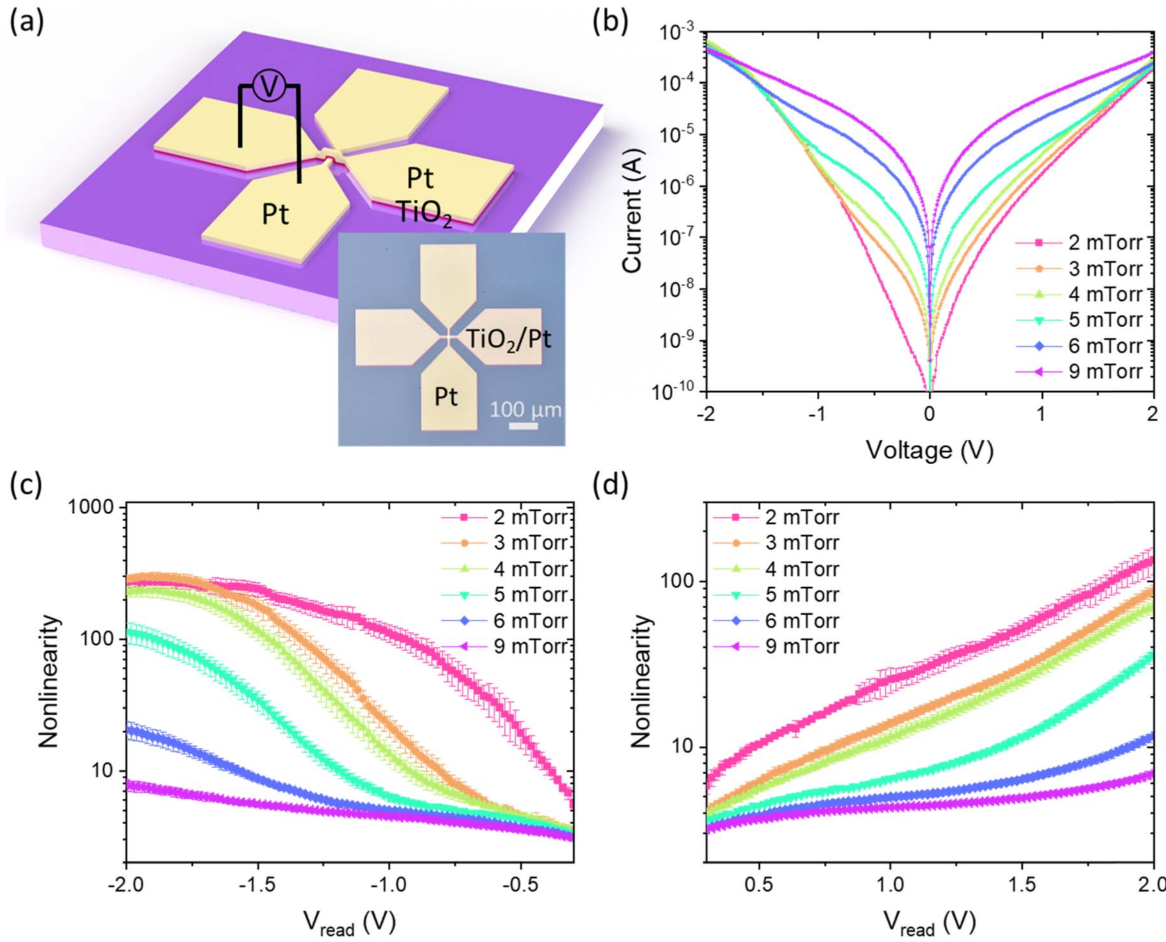

Figure 2. (a) Schematic illustration of the $Pt/TiO_2/Pt$ exponential selector device. Inset in panel (a) shows the optical image of the device. (b) *I–V* characteristics of the $Pt/TiO_2/Pt$ selector deposited under different sputtering pressures. Nonlinearity versus reading voltage of $Pt/TiO_2/Pt$ selector for (c) negative and (d) positive voltage biases.

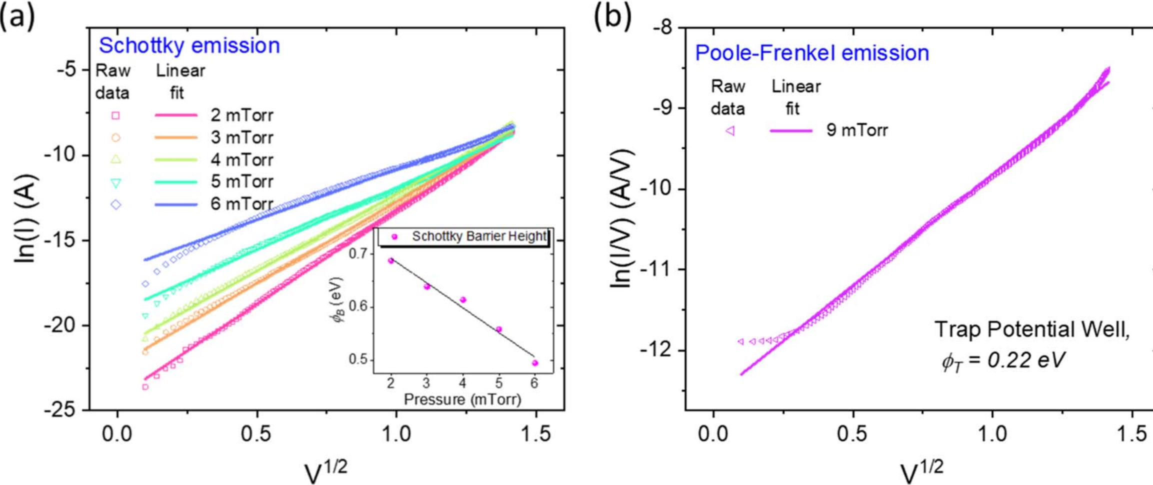

Figure 3. (a) Ln(I) versus $V^{1/2}$ plot in the positive voltage region for Schottky emission fitting. The inset in (a) shows the SBH of the selectors from 2 to 6 mTorr. (b) Ln(I/V) versus $V^{1/2}$ plot in the positive voltage region for Poole–Frenkel emission fitting.

be expressed as [33–35]

$$J_{\mathrm{PF}} = q\mu N_c E \exp\left[\frac{-q(\phi_T - \sqrt{qE/\pi\varepsilon})}{kT}\right], \quad (2)$$

where ϕ_T is the trap potential well and N_c is the density of states in the conduction band of the oxide. It is important to note that Schottky emission is an interface-limited conduction mechanism, while Poole–Frenkel emission is a bulk-limited conduction mechanism.

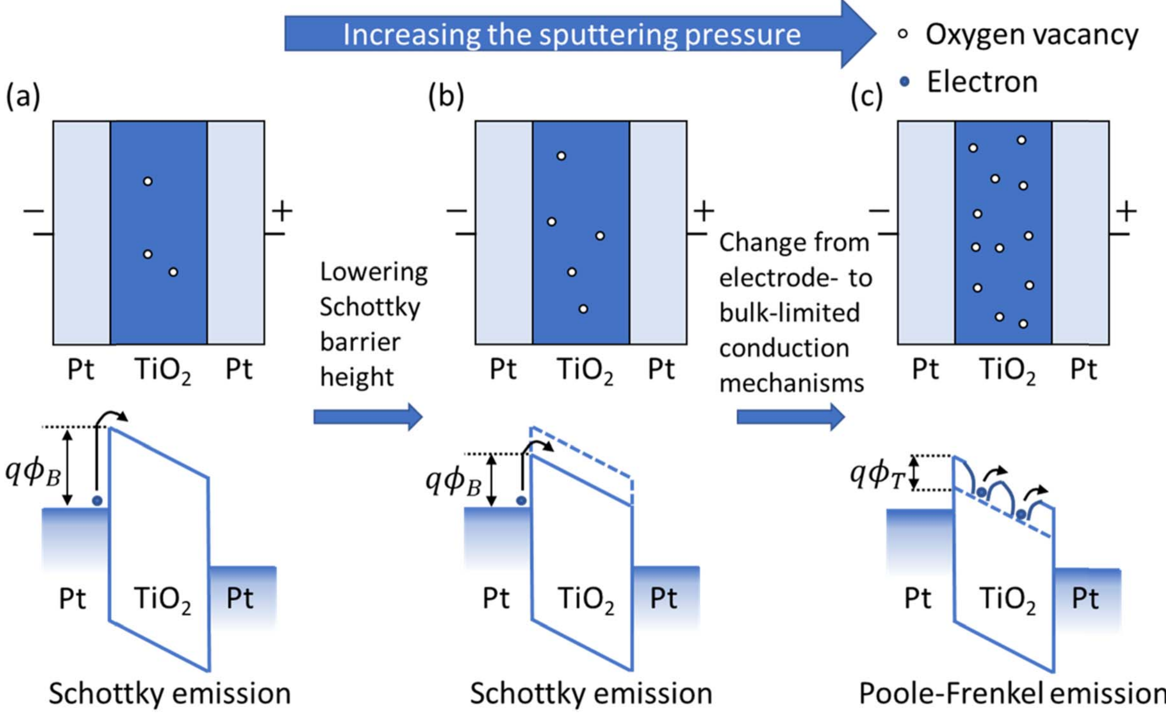

Figure 4. Schematic of the proposed conduction mechanism transition of the $Pt/TiO_2/Pt$ structure based on the concentration of oxygen vacancy defects in the TiO_2 layer.

To explain the conduction mechanism transition of the $Pt/TiO_2/Pt$ structure, a transition model based on the concentration of oxygen vacancy defects in the TiO_2 layer is proposed, as shown in figure 4. At low sputtering pressure (2 mTorr), the concentration of oxygen vacancy defects in the device is low. Thus, most of the conduction electrons come from the electrons in the metal that are thermally activated to overcome the energy barrier into the conduction band of the TiO_2 layer, and the dominant conduction mechanism is Schottky emission, as shown in figure 4(a). When the sputtering pressure increases (from 2 to 6 mTorr), the oxygen vacancy defect concentration in the oxide increases, as shown in figure 4(b). Furthermore, the number of defects at the metal/oxide interface tends to be larger when there are more defects in the bulk [36]. When there are more defects at the metal/oxide interface, the SBH tends to become smaller due to image force [30, 33]. Therefore, the SBH decreases from 2 to 6 mTorr devices, as shown in the inset of figure 3(a). When the sputtering pressure further increases, the oxygen vacancy defect density increases significantly, as shown in figure 4(c). The oxygen vacancies can act as trapping centres for electrons [37]. As there are more electrons in the oxygen vacancy traps, the number of electrons thermally excited from traps into the conduction band of the TiO_2 layer also increases. Consequently, the number of electrons emitted from traps into the conduction band of the TiO_2 layer exceeds the number of electrons emitted from metal into the conduction band of the TiO_2 layer. As a result, the dominant conduction mechanism transits from Schottky emission, which is an interface-limited conduction mechanism, to Poole–Frenkel emission, which is a bulk-limited conduction mechanism with increasing sputtering pressure.

Figure 5 shows the short-term plasticity of the $Pt/TiO_2/Pt$ exponential selector. One hundred pulses at $+2$ V and -2 V with 10 μs pulse width for different pulse intervals were applied to the 2 mTorr $Pt/TiO_2/Pt$ exponential selector, as shown in figures 5(a) and (b), respectively. The current (conductance) of the selector decreases when $+2$ V pulses are applied, while the current increases when -2 V pulses are applied. Additionally, when the pulse interval decreases, the volatile current change increases for both polarity pulses. It is important to note that the conductance of the selector relaxes back to the initial state after the removal of the voltage pulses.

To investigate the impact of oxide and defect densities on the short-term plasticity of the $Pt/TiO_2/Pt$ exponential selector, the current change under one hundred pulses with a pulse interval of 100 ns was measured from five devices for each pressure, as shown in figure 5(c). The magnitude of current change decreases with increasing pressure for both polarity pulses, which indicates that the short-term plasticity feature is enhanced with lower sputtering pressure. Additionally, the relaxation behaviours of the $Pt/TiO_2/Pt$ exponential selector under different pressures are investigated, as shown in figure 5(d). After the one hundred pulses, a 2 s relaxation duration is implemented and a voltage pulse of 2 V or -2 V is applied to the selector, as shown in the supplementary information (figures S4 and S5). Under negative voltage pulses, all selectors from 2 to 9 mTorr pressure show short-term plasticity features. Whereas, under positive voltage pulses, only selectors from 2 to 4 mTorr show short-term plasticity features. The selector with 5 mTorr pressure shows half short-term and half long-term plasticity features as the measured current relax halfway back to the initial value. On

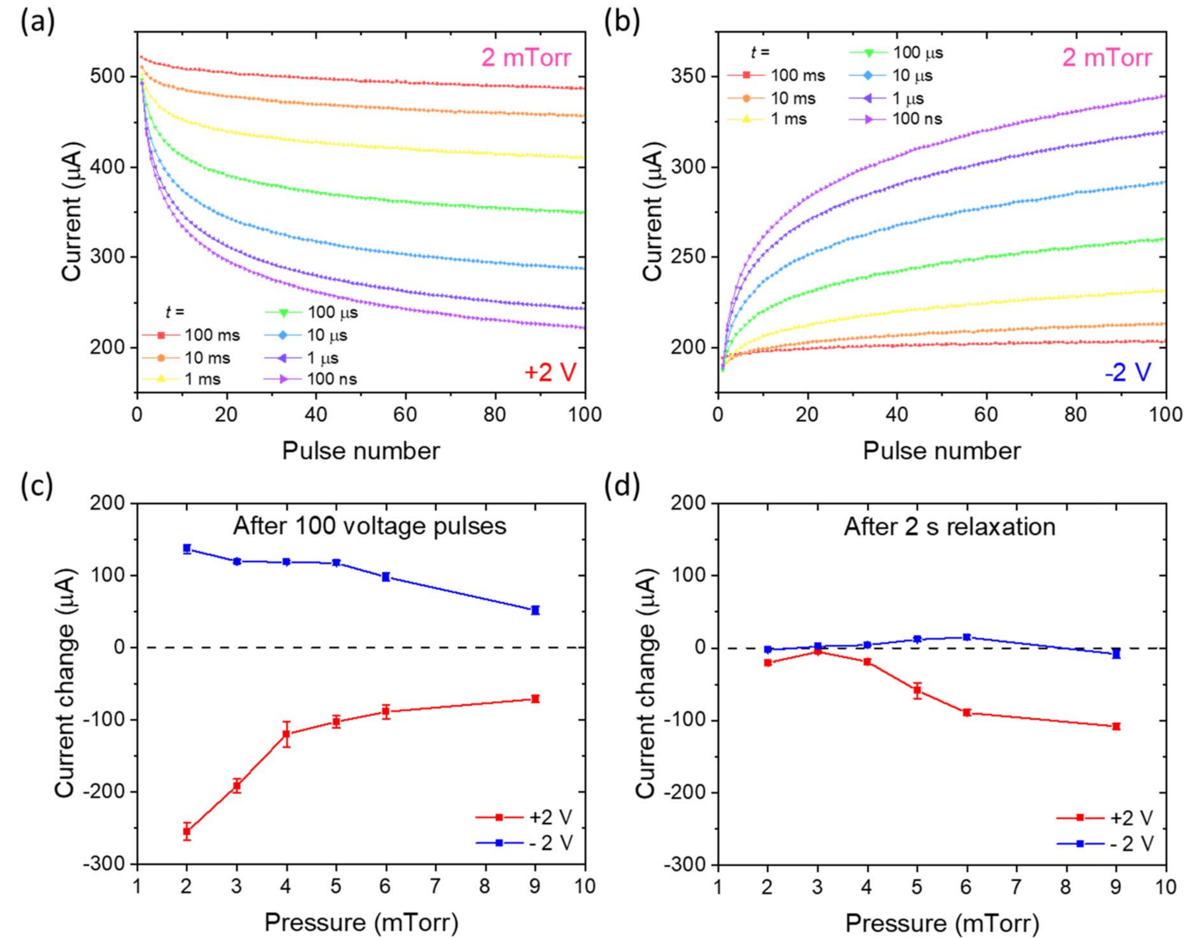

Figure 5. Short-term plasticity of the Pt/TiO_2/Pt selector with 2 mTorr sputtering pressure under (a) +2 V and (b) −2 V pulses with 10 μs pulse width for various pulse intervals. Measured current change with a pulse interval of 100 ns for various pressures (c) after one hundred pulses and (d) after 2 s of relaxation duration.

the other hand, the selectors with 6 and 9 mTorr pressure show long-term plasticity features as the measured current retains after a 2 s relaxation period. The relaxation behaviour as a function of time of the selector is also studied as shown in the supplementary information (figures S6 and S7). The result agrees with the measurement as shown in figure 5(d), where the devices relax slower back to the initial state as the sputtering pressure increases. In addition, the 2 mTorr device decays back to the initial state at ∼500 ms for both positive and negative voltages, as shown in the supplementary information (figure S8).

In our previous work, the short-term plasticity of the Pt/TiO_2/Pt exponential selector can be explained by the drift and diffusion of mobile Ti^{3+} and O^{2-} ions at positive and negative voltages, respectively [18]. As the sputtering pressure increases, the composition of non-lattice oxygen increases. The increase of non-lattice oxygen composition could restrain the electromigration of Ti^{3+} and O^{2-} ions in the TiO_2 layer, which results in decreasing current change under one hundred pulses with pressure, as shown in figure 5(c). Besides that, as the sputtering pressure increases, the increasing electromigration restriction causes the selector device to relax slower back to the initial state, as shown in the supplementary information (figure S6). Additionally, the transition from short-term to long-term plasticity for positive voltage, as shown in figure 5(d), could be ascribed to the increase in the composition of non-lattice oxygens. The Ti^{3+} cations could not be diffused back to the initial position due to the blocking of abundant non-lattice oxygens in high sputtering pressure selectors, which results in long-term plasticity. Thus, to achieve a remarkable short-term plasticity feature, it is important to fabricate the selector device at low sputtering pressure.

4. Conclusion

In summary, the Pt/TiO_2/Pt exponential selectors with different oxide and defect densities were fabricated by controlling the sputtering pressures. *I–V* measurements reveal that the selector with a lower defect density exhibits a higher nonlinearity. The dominant conduction mechanisms for the Pt/TiO_2/Pt structures are found to be Schottky emission and Poole–Frenkel emission at low defect densities and high defect densities, respectively. For sputtering pressure less than 6 mTorr, the SBH decreases with increasing oxygen vacancy defect density. A model is also given to explain the dominant conduction mechanism transition from Schottky emission to Poole–Frenkel emission based on the concentration of oxygen

vacancies in the TiO_2 layer. Additionally, the selector device with a lower defect density shows a bigger current change for the short-term plasticity feature. These results suggest that it is helpful to fabricate the $Pt/TiO_2/Pt$ exponential selector at the lowest possible pressure to achieve the highest nonlinearity and the most prominent short-term plasticity characteristic.

The short-term plasticity $Pt/TiO_2/Pt$ exponential selector can be further optmised for the applications in very large scale 1S1R crossbar array. The main challenge of the $Pt/TiO_2/Pt$ selector is the medium nonlinearity (5×10^3 in the $V/3$ scheme) of the selector. This could be possibly overcome by changing the electrode materials or designing a complex multi-layer oxide structure. On the other hand, the main advantage of employing the $Pt/TiO_2/Pt$ selector is that the temporal processing capability of the 1S1R synaptic device can be granted by the short-term plasticity feature of the selector. This enables the 1S1R synapse to differentiate and register the stimulation rate of the input signal in the crossbar array without requiring the RRAM or other memristor devices (e.g. PCM) to possess short-term plasticity features. This 1S1R integration permits the memristive device to develop in other aspects, such as multilevel capability and high endurance. In addition, the 1S1R synapse could be modulated to be more sensitive to a certain range of stimulation rates with the tunable short-term plasticity feature of the selector. Therefore, the tunable short-term plasticity $Pt/TiO_2/Pt$ exponential selector is handy to be implemented in 1S1R crossbar arrays for neuromorphic computing applications.

Acknowledgments

This work was supported by a RIE2020 ASTAR AME IAF-ICP Grant (No. I1801E0030).

Data availability statement

All data that support the findings of this study are included within the article (and any supplementary files).

ORCID iDs

Mun Yin Chee https://orcid.org/0000-0002-1580-1463
Putu Andhita Dananjaya https://orcid.org/0000-0001-9416-6455
Gerard Joseph Lim https://orcid.org/0000-0003-2411-5841
Calvin Xiu Xian Lee https://orcid.org/0000-0002-5426-2482
Lingli Liu https://orcid.org/0000-0002-4360-2699
Wen Siang Lew https://orcid.org/0000-0002-5161-741X

References

[1] Wan W *et al* 2022 A compute-in-memory chip based on resistive random-access memory *Nature* **608** 504–12
[2] Wang Z *et al* 2018 Capacitive neural network with neuro-transistors *Nat. Commun.* **9** 3208
[3] Hou K, Chen S, Zhou C, Nguyen L L, Dananjaya P A, Duchamp M, Bazan G C, Lew W S and Leong W L 2021 Operando direct observation of filament formation in resistive switching devices enabled by a topological transformation molecule *Nano Lett.* **21** 9262–9
[4] Dananjaya P A, Loy D J J, Chow S C W and Lew W S 2019 Unidirectional threshold switching induced by Cu migration with high selectivity and ultralow OFF current under gradual electroforming treatment *ACS Appl. Electron. Mater.* **1** 2076–85
[5] Upadhyay N K, Blum T, Maksymovych P, Lavrik N V, Davila N, Katine J A, Ievlev A V, Chi M, Xia Q and Yang J J 2021 Engineering tunneling selector to achieve high nonlinearity for 1S1R integration *Front. Nanotechnol.* **3** 656026
[6] Cortese S, Khiat A, Carta D, Light M E and Prodromakis T 2016 An amorphous titanium dioxide metal insulator metal selector device for resistive random access memory crossbar arrays with tunable voltage margin *Appl. Phys. Lett.* **108** 33505
[7] Kim Y, Kwon Y J, Kim J, An C H, Park T, Kwon D E, Woo H C, Kim H J, Yoon J H and Hwang C S 2019 Novel selector-induced current-limiting effect through asymmetry control for high-density one-selector–one-resistor crossbar arrays *Adv. Electron. Mater.* **5** 1800806
[8] Huang J-J, Tseng Y-M, Hsu C-W and Hou T-H 2011 Bipolar nonlinear $Ni/TiO/Ni$ selector for 1S1R crossbar array applications *IEEE Electron Device Lett.* **32** 1427–9
[9] Shin J, Choi G, Woo J, Park J, Park S, Lee W, Kim S, Son M and Hwang H 2012 MIM-type cell selector for high-density and low-power cross-point memory application *Microelectron. Eng.* **93** 81–4
[10] Lee W *et al* 2012 High current density and nonlinearity combination of selection device based on $TaO_x/TiO_2/TaO_x$ structure for one selector–one resistor arrays *ACS Nano* **6** 8166–72
[11] Woo H C, Kim J, Lee S, Kim H J and Hwang C S 2022 Stacked one-selector-one-resistive memory crossbar array with high nonlinearity and on-current density for the neuromorphic applications *Adv. Electron. Mater.* **8** 2200656
[12] Wang M, Zhou J, Yang Y, Gaba S, Liu M and Lu W D 2015 Conduction mechanism of a TaO_x-based selector and its application in crossbar memory arrays *Nanoscale* **7** 4964–70
[13] Wang R, Shi T, Zhang X, Wu Z and Liu Q 2021 A dual-functional $Ta/TaO_x/Ru$ device with both nonlinear selector and resistive switching behaviors *RSC Adv.* **11** 18241–5
[14] Kumar D, Aluguri R, Chand U and Tseng T-Y 2019 One bipolar selector-one resistor for flexible crossbar memory applications *IEEE Trans. Electron Devices* **66** 1296–301
[15] Kim K H, Seo M-J and Jang B C 2023 Amorphous ITZO-based selector device for memristor crossbar array *Micromachines* **14** 506
[16] Wang C-H, Chen V, McClellan C J, Tang A, Vaziri S, Li L, Chen M E, Pop E and Wong H-S P 2021 Ultrathin three-monolayer tunneling memory selectors *ACS Nano* **15** 8484–91
[17] Du C, Cai F, Zidan M A, Ma W, Lee S H and Lu W D 2017 Reservoir computing using dynamic memristors for temporal information processing *Nat. Commun.* **8** 2204
[18] Chee M Y, Dananjaya P A, Lim G J, Du Y and Lew W S 2022 Frequency-dependent synapse weight tuning in 1S1R with a short-term plasticity TiO_x−based exponential selector *ACS Appl. Mater. Interfaces* **14** 35959–68
[19] Shin S *et al* 2022 Emulating the short-term plasticity of a biological synapse with a ruthenium complex-based organic mixed ionic-electronic conductor *Mater. Adv.* **3** 2827–37
[20] Lee Y, Mahata C, Kang M and Kim S 2021 Short-term and long-term synaptic plasticity in $Ag/HfO_2/SiO_2/Si$ stack by

controlling conducting filament strength *Appl. Surf. Sci.* **565** 150563

[21] Parratt L G 1954 Surface studies of solids by total reflection of x-rays *Phys. Rev.* **95** 359–69

[22] Névot L and Croce P 1980 Caractérisation des surfaces par réflexion rasante de rayons X. application à l'étude du polissage de quelques verres silicates *Rev. Phys. Appl.* **15** 761–79

[23] Lee C, Choi W, Kwak M, Kim S and Hwang H 2021 Impact of electrolyte density on synaptic characteristics of oxygen-based ionic synaptic transistor *Appl. Phys. Lett.* **119** 103503

[24] Ghenzi N, Rozenberg M J, Llopis R, Levy P, Hueso L E and Stoliar P 2015 Tuning the resistive switching properties of TiO_{2-x} films *Appl. Phys. Lett.* **106** 123509

[25] Eufinger K, Janssen E N, Poelman H, Poelman D, De Gryse R and Marin G B 2006 The effect of argon pressure on the structural and photocatalytic characteristics of TiO_2 thin films deposited by d.c. magnetron sputtering *Thin Solid Films* **515** 425–9

[26] Ding X, Feng Y, Huang P, Liu L and Kang J 2019 Low-power resistive switching characteristic in HfO_2/TiO_x Bi-layer resistive random-access memory *Nanoscale Res. Lett.* **14** 157

[27] Yang M K, Kim G H, Ju H, Lee J-K and Ryu H-C 2015 An analysis of 'non-lattice' oxygen concentration effect on electrical endurance characteristic in resistive switching MnO_x thin film *Appl. Phys. Lett.* **106** 53504

[28] Ide K, Nomura K, Hosono H and Kamiya T 2019 Electronic defects in amorphous oxide semiconductors: a review *Phys. Status Solidi* **216** 1800372

[29] Jeong J H, Yang H W, Park J-S, Jeong J K, Mo Y-G, Kim H D, Song J and Hwang C S 2008 Origin of subthreshold swing improvement in amorphous indium gallium zinc oxide transistors *Electrochem. Solid-State Lett.* **11** H157

[30] Lim E W and Ismail R 2015 Conduction mechanism of valence change resistive switching memory: a survey *Electron* **4** 586–613

[31] Martinez-Lopez A G, Padron-Hernandez W Y, Pourjafari D, Oskam G, Rodriguez-Gattorno G, Estrada M and Tinoco J C 2018 Electrical characterization of schottky diodes based on inkjet-printed TiO_2 films *IEEE Electron Device Lett.* **39** 1940–3

[32] Alamgir Z, Beckmann K, Holt J and Cady N C 2017 Pulse width and height modulation for multi-level resistance in bi-layer TaO_x based RRAM *Appl. Phys. Lett.* **111** 63111

[33] Chiu F-C 2014 A review on conduction mechanisms in dielectric films *Adv. Mater. Sci. Eng.* **2014** 578168

[34] Yang H, Jain M, Suvorova N A, Zhou H, Luo H M, Feldmann D M, Dowden P C, DePaula R F, Foltyn S R and Jia Q X 2007 Temperature-dependent leakage mechanisms of $Pt/BiFeO_3/SrRuO_3$ thin film capacitors *Appl. Phys. Lett.* **91** 72911

[35] Pabst G W, Martin L W, Chu Y-H and Ramesh R 2007 Leakage mechanisms in $BiFeO_3$ thin films *Appl. Phys. Lett.* **90** 72902

[36] Lau W S 2012 An extended unified schottky-poole-frenkel theory to explain the current-voltage characteristics of thin film metal-insulator-metal capacitors with examples for various high-*k* dielectric materials *ECS J. Solid State Sci. Technol.* **1** N139–48

[37] Papageorgiou A C, Beglitis N S, Pang C L, Teobaldi G, Cabailh G, Chen Q, Fisher A J, Hofer W A and Thornton G 2010 Electron traps and their effect on the surface chemistry of $TiO_2(110)$ *Proc. Natl Acad. Sci.* **107** 2391–6